Nanoscale Res Lett (2009) 4:90–93
DOI 10.1007/s11671-008-9207-4

NANO EXPRESS

# The Effect of Interface Texture on Exchange Biasing in $Ni_{80}Fe_{20}/Ir_{20}Mn_{80}$ System

**Yuan-Tsung Chen**

Received: 23 July 2008 / Accepted: 11 November 2008 / Published online: 25 November 2008


**Abstract** Exchange-biasing phenomenon can induce an evident unidirectional hysteresis loop shift by spin coupling effect in the ferromagnetic (FM)/antiferromagnetic (AFM) interface which can be applied in magnetoresistance random access memory (MRAM) and recording-head applications. However, magnetic properties are the most important to AFM texturing. In this work, top-configuration exchange-biasing NiFe/IrMn($x$ Å) systems have been investigated with three different conditions. From the high-resolution cross-sectional transmission electron microscopy (HR X-TEM) and X-ray diffraction results, we conclude that the IrMn (111) texture plays an important role in exchange-biasing field ($H_{ex}$) and interfacial exchange energy ($J_k$). $H_{ex}$ and $J_k$ tend to saturate when the IrMn thickness increases. Moreover, the coercivity ($H_c$) dependence on IrMn thickness is explained based on the coupling or decoupling effect between the spins of the NiFe and IrMn layers near the NiFe/IrMn interface. In this work, the optimal values for $H_{ex}$ and $J_k$ are 115 Oe and 0.062 erg/cm$^2$, respectively.

**Keywords** Exchange biasing · Texture · Coupling or decoupling effect

## Introduction

The exchange-biasing phenomenon using the IrMn basing layer can be applied in magnetoresistance random access memory (MRAM) and recording-head applications extensively because $Ir_{20}Mn_{80}$ exhibits great characteristics: high interfacial exchange energy ($J_k$) (or exchange-biasing field ($H_{ex}$)), low coercivity ($H_c$), high blocking temperature ($T_B$), and good thermal stability in device performance [1–5]. Moreover, the NiFe/IrMn also can be applied in the high-frequency ferromagnetic resonance (FMR) [6]. In a ferromagnetic (FM)/antiferromagnetic (AFM) system, the texturing in the AFM layer can have an important impact on the magnetic properties of the system. In the past, a NiO/NiFe system with varied AFM NiO thicknesses was studied [7]. In this paper, we will show how the magnetic properties, such as $H_{ex}$, $H_c$, and $J_k$, of the IrMn/NiFe top-configuration system may vary as a function of the IrMn layer thickness ($x$). It is found that these magnetic properties are closely related to the degree of the (111) texture in the IrMn layer [8–10]. $H_{ex}$ and $J_k$ tend to saturate as $x$ increases beyond 90 Å. $H_c$ is inversely proportional to $x$, which is caused by the spin coupling or decoupling effect near the NiFe/IrMn interface.

## Experiment Details

The top-configuration NiFe/IrMn system was made by DC magnetron sputtering onto a glass substrate. The deposition sequences were: glass/Ta(30 Å)/NiFe(50 Å)/IrMn($x$ Å)/Ta(100 Å), where $x$ = 15, 30, 60, 90, 110, and 150 Å. For this system, we have applied three different conditions during and/or after deposition: (a) the substrate temperature ($T_s$) was kept at room temperature (RT) only; (b) $T_s$ was at RT with an in-plane external field (h) = 500 Oe during deposition; and (c) $T_s$ = RT, with h during deposition and post-deposition annealing in the field at $T_A$ = 250 °C for 1 h, and then field-cooling to RT. The seed Ta layer was

Y.-T. Chen (✉)
Department of Materials Science and Engineering, I-Shou University, No. 1, Sec. 1, Syuecheng Road, Dashu Township, Kaohsiung 840, Taiwan, Republic of China
e-mail: ytchen@isu.edu.tw

used in order to induce a stronger (111) texture in the NiFe or IrMn layer [3]. The cap Ta layer was used to protect the IrMn layer from oxidation. The target compositions of the IrMn and NiFe alloy are 20 at.% Ir, 80 at.% Mn and 80 at.% Ni, 20 at.% Fe, respectively. The typical base chamber pressure was better than $1 \times 10^{-7}$ Torr, and the Ar working chamber pressure was $5 \times 10^{-3}$ Torr.

The degree of the (111) texture of the $Ir_{20}Mn_{80}$ layer was characterized by the X-ray diffraction method using a $CuK_{\alpha 1}$ line. In order to observe the growth texture and the interfacial morphology directly, we performed high-resolution cross-sectional transmission electron microscopy (HR X-TEM). The exchange-biased magnetic hysteresis loop was measured by a LakeShore Model 7300 vibrating sample magnetometer (VSM).

## Results and Discussion

Figure 1 shows a typical unidirectional shifted hysteresis loop for the top-configuration NiFe(50 Å)/IrMn(90 Å) sample grown under condition (c). From this figure $H_{ex}$ and $H_c$ are defined: i.e., $H_{ex} \equiv (H_1 + H_2)/2$ and $H_c \equiv (H_1 - H_2)/2$. We find that $H_{ex} = 112$ Oe and $H_c = 42$ Oe in this sample.

Figure 2 shows the X-TEM images of the three NiFe(50 Å)/IrMn(90 Å) samples made under three different conditions, from (a) to (c), respectively. In Fig. 2a, the IrMn (111) crystal plane has grown randomly on the underneath NiFe layer. This indicates that condition (a) is not sufficient to induce the stronger IrMn texture. Under condition (b), as shown in Fig. 2b, the (111) texture arrangement seems better than that in Fig. 2a, but it is still not the best. In contrast, condition (c) can induce an almost perfect IrMn (111) texturing, which follows the underlying NiFe (111) growth texture closely. This clearly indicates that the (111) texturing can cross the NiFe/IrMn interface when $T_A$ is raised to 250 °C. In short, the post-annealing at elevated $T_A$ and the deposition field h are necessary conditions to produce the strongest IrMn (111) texture in the NiFe/IrMn system.

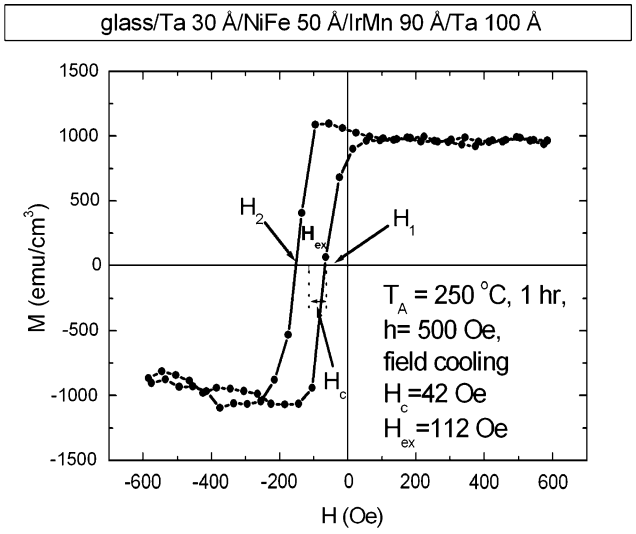


**Fig. 1** The hysteresis loop of a glass/Ta(30 Å)/NiFe(50 Å)/IrMn(90 Å)/Ta(100 Å) sample. This sample was post-annealed at $T_A = 250$ °C and $h = 500$ Oe for 1 h and then field-cooled to RT. The switching fields $H_1$ and $H_2$, exchange-biasing field ($H_{ex}$), and coercivity ($H_c$) are indicated in the figure

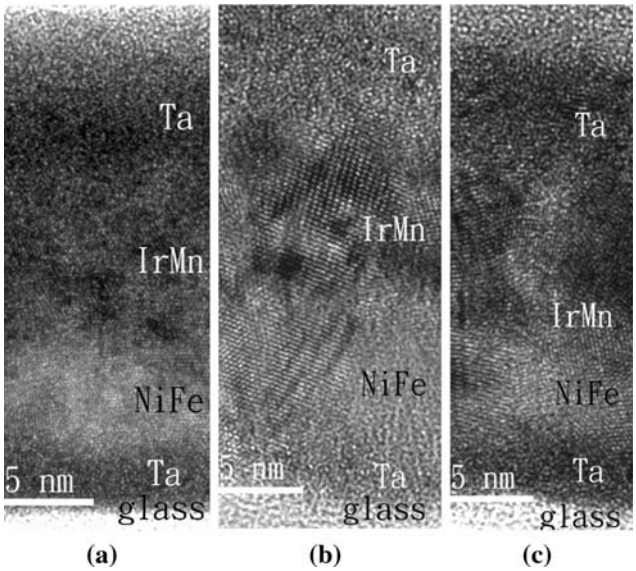


**Fig. 2** The X-TEM images of glass/Ta(30 Å)/NiFe(50 Å)/IrMn(90 Å)/Ta(100 Å) samples under three different deposition conditions: **a** deposited at RT only, **b** deposited at RT with an external field $h = 500$ Oe, and **c** the same film-growth procedure as in (**b**), post-annealing at $T_A = 250$ °C with $h$ on for 1 h, and then field-cooling to RT

Figure 3 shows different degrees of the IrMn (111) texture in the NiFe(50 Å)/IrMn($x$) system with X-ray diffraction. $I_o$ is the intensity of the IrMn (111) line and $I_b$ is the background intensity. According to this figure, there is a higher IrMn (111) texture in conditions (b) or (c). As to condition (a) in Fig. 3, the (111) texture is clearly not well developed yet. These phenomena are consistent with the results from X-TEM images.

Figure 4 shows $H_{ex}$ plotted as a function of the IrMn thickness ($x$) for the NiFe(50 Å)/IrMn($x$) system under various conditions. As $x \leq 15$ Å, there is almost no exchange-bias interaction, since $J_k > K_{AF}x$, where $K_{AF}$ is the anisotropy energy of IrMn [10]. When $x$ increases from 15 Å to 60 Å, the IrMn pinning action becomes more effective, or $J_k = K_{AF}x$, which indicates that $H_{ex}$ should increase with increasing $x$. Moreover, we find that as $x \geq 90$ Å under conditions (a)–(c), $H_{ex}$ tends to saturate. The last phenomenon is consistent with X-ray and X-TEM results indicating that the continuation of the (111)

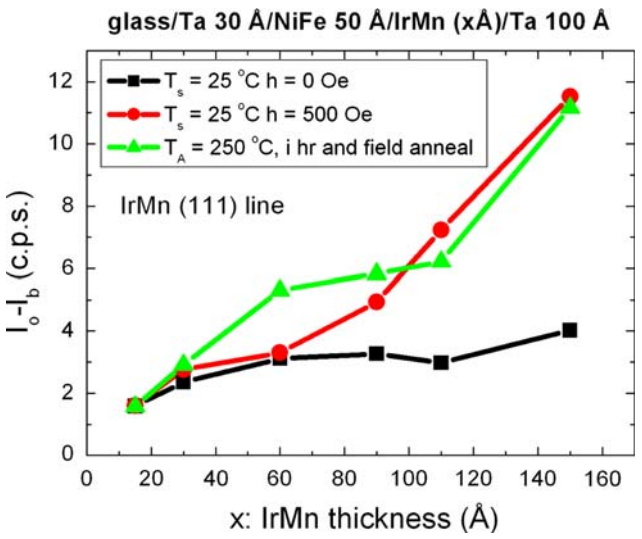


**Fig. 3** The degree of the IrMn (111) texture, as determined from the X-ray diffraction studies, is shown as a function of $x$ for glass/Ta(30 Å)/NiFe(50 Å)/IrMn($x$ Å)/Ta(100 Å). $I_o$ is the intensity of the IrMn (111) line and $I_b$ is the background intensity

perpendicular texture across the NiFe/IrMn interface should stop $H_{ex}$ from decreasing.

According to the well-known theory based on the interfacial exchange-biasing phenomenon,

$$J_k = H_{ex} M_s t_{FM} \quad (1)$$

where $M_s$ is the saturation magnetization of the NiFe layer. Since the ferromagnetic thickness $t_{FM} = 50$ Å is fixed for these NiFe/IrMn systems, $M_s$ is constant. Therefore, from Eq. 1, $J_k$ is proportional to $H_{ex}$. The $x$ dependence of $J_k$ in

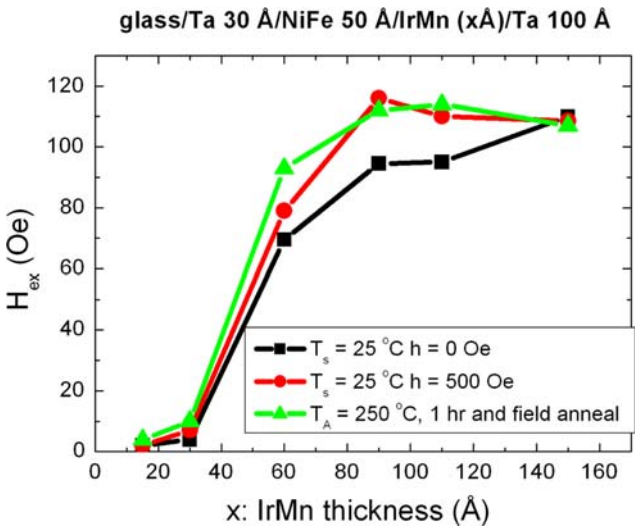


**Fig. 4** IrMn thickness ($x$) dependence of the exchange-biasing field ($H_{ex}$) for the glass/Ta(30 Å)/NiFe(50 Å)/IrMn($x$ Å)/Ta(100 Å) samples under conditions (**a**) to (**c**)

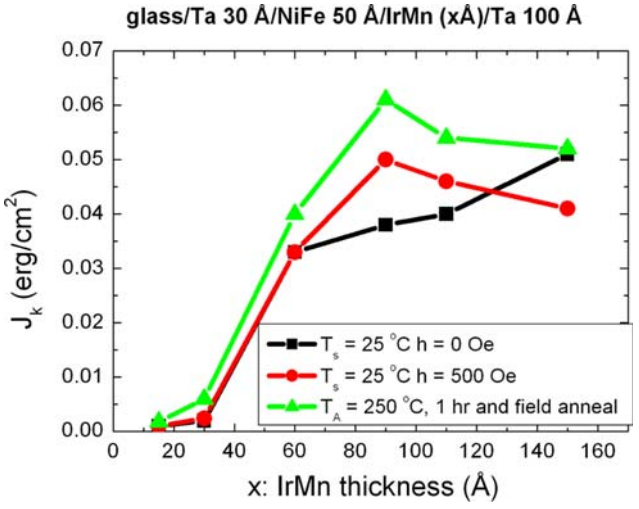


**Fig. 5** IrMn thickness ($x$) dependence of the interfacial energy ($J_k$) is shown for the glass/Ta(30 Å)/NiFe(50 Å)/IrMn($x$)/Ta(100 Å) systems

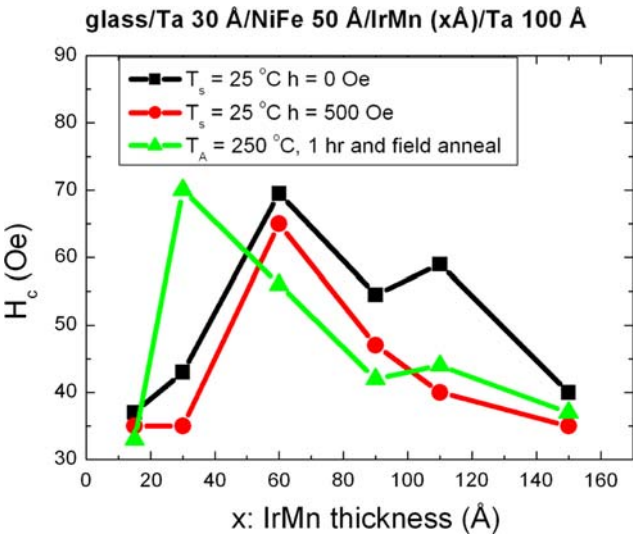


**Fig. 6** Coercivity ($H_c$) versus the IrMn thickness ($x$) for the glass/Ta(30 Å)/NiFe(50 Å)/IrMn ($x$ Å)/Ta(100 Å) systems

Fig. 5 should look similar to that of $H_{ex}$ in Fig. 4. Note that the largest $J_k$ value, about 0.062 erg/cm$^2$, has been realized in this study, as shown in Fig. 5. The value is about half of that found in reference [11].

The $H_c$ is plotted as a function of $x$ in Fig. 6. In general, $H_c$ increases in the $x$ range from 15 Å to 30 Å (or 60 Å) and decreases in the $x$ range thereafter. According to reference [12], the $H_c$ behaviors are caused by the spin coupling and decoupling effects at the NiFe/IrMn interface as $x$ increases. As discussed before, when $x$ increases from 30 Å to 60 Å, $H_{ex}$ increases gradually, which implies the NiFe/IrMn coupling drag interaction. In turn, the coupling force between the NiFe and the nearest IrMn spins at the

interface is larger than that between neighboring IrMn spins. The external field ($H$) needs to rotate not only the NiFe spins but also the IrMn spins on top together. As a result, the resistance to domain wall motion is higher, and $H_c$ should increase as $x$ increases from 15 Å to 60 Å. However, as $x$ continues to increase, $H_c$ eventually decreases, due to the decoupling effect between the interfacial NiFe spin and the IrMn spin on top. The reason for the decoupling is that as $x$ continues to increase, $H_{ex}$ is fully developed, and even the lowest-level IrMn spin (at the interface) is strongly pinned by the IrMn spins above. Therefore, when the external field is large enough to switch the NiFe spin at $H = H_c$, the neighboring IrMn spin does not rotate together anymore. Hence, $H_c$ decreases as $x \geq 60$ Å (Fig. 6).

## Conclusions

In conclusion, under the various conditions (a)–(c) for the top-configuration NiFe/IrMn systems, the magnetic properties, such as $H_{ex}$, $J_k$, and $H_c$, have been investigated. These magnetic properties are closely related to the growth IrMn (111) texturing. From HR X-TEM and X-ray diffraction results, we conclude that the strongest IrMn (111) texture appears in condition (c). Therefore, condition (c) should induce the highest $H_{ex}$ and $J_k$. Furthermore, the $H_c$ value first increases and then decreases as $x$ increases from 15 Å to 150 Å. This is due to the spin coupling and decoupling drag effects at the NiFe/IrMn interfaces. The optimal $H_{ex}$ and $J_k$ values obtained from this study are 115 Oe and 0.062 erg/cm$^2$, respectively. This $H_{ex}$ value of NiFe/IrMn is larger or equal to the optimal $H_{ex}$ in the NiO/NiFe systems [13, 14].

**Acknowledgments** This work was supported by the National Science Council and I-Shou University, under Grant Nos. (NSC97-2112-M214-001-MY3), (ISU97-S-03), and (ISU97-02-20).

## References

1. C.C.Y. Andrew, X.F. Han, J. Murai, Y. Ando, T. Miyazaki, K. Hiraga, J. Magn. Magn. Mater. **240**, 130 (2002). doi:10.1016/S0304-8853(01)00734-X
2. D. Lacour, O. Durand, J.-L. Maurice, H. Jaffrès, F. Nguyen Van Dau, F. Petroff, P. Etienne, J. Humbert, A. Vaurès, J. Magn. Magn. Mater. **270**, 403 (2004). doi:10.1016/j.jmmm.2003.09.007
3. L. Hua-Rui, R. Tian-Ling, Q. Bin-Jun, L. Li-Tian, K. Wan-Jun, L. Wei, Thin Solid Films **441**, 111 (2003). doi:10.1016/S0040-6090(03)00952-0
4. J. van Driel, F.R. de Boer, K.-M.H. Lenssen, R. Coehoorn, J. Appl. Phys. **88**, 975 (2000). doi:10.1063/1.373764
5. S.-F. Cheng, P. Lubitz, J. Appl. Phys. **87**, 4927 (2000). doi:10.1063/1.373205
6. O. Acher, S. Queste, K.-U. Barholz, R. Mattheis, J. Appl. Phys. **93**, 6668 (2003). doi:10.1063/1.1556098
7. C.H. Lai, H. Matsuyama, R.L. White, T.C. Anthony, G.G. Bush, J. Appl. Phys. **79**, 6389 (1996). doi:10.1063/1.362007
8. P. Wisniowski, T. Stobiecki, J. Kanak, G. Reiss, H. Bruckl, J. Appl. Phys. **100**, 13906 (2006). doi:10.1063/1.2209180
9. A.E. Berkowitz, Kentaro. Takano, J. Magn. Magn. Mater. **200**, 552 (1999). doi:10.1016/S0304-8853(99)00453-9
10. G. Malinowski, M. Hehn, S. Robert, O. Lenoble, A. Schuhl, J. Appl. Phys. **98**, 113903 (2005). doi:10.1063/1.2136233
11. Y.T. Chen, S.U. Jen, Y.D. Yao, J.M. Wu, J.H. Liao, T.B. Wu, J. Alloy. Compd. **448**, 59 (2008). doi:10.1016/j.jallcom.2006.12.099
12. M. Ali, C.H. Marrows, M. Al-Jawad, B.J. Hickey, A. Misra, U. Nowak, K.D. Usadel, Phys. Rev. B **68**, 214420 (2003). doi:10.1103/PhysRevB.68.214420
13. G.H. Yu, C.L. CHai, H.C. Zhao, F.W. Zhu, J.M. Xiao, J. Magn. Magn. Mater. **224**, 61 (2001). doi:10.1016/S0304-8853(00)01337-8
14. D.G. Huang, C.M. Park, S.S. Lee, J. Magn. Magn. Mater. **186**, 265 (1998). doi:10.1016/S0304-8853(98)00089-4